Time-Resolved SAXS Studies on Crystallization Behavior of Poly(ethylene isophthalate-*co*-ethylene terephthalate)s

*B. Lee, T. J. Shin, S. W. Lee, J.W. Lee, M. Ree**

Pohang University of Science and Technology, Department of Chemistry, Center for Integrated Molecular Systems, BK21 Functional Polymer Thin Group, Polymer Research Institute and Pohang Accelerator Laboratory
San 31, Hyoja-dong, Pohang 790-784, Republic of Korea

SUMMARY: Small-angle X-ray scattering measurements using synchrotron radiation were carried out for poly(ethylene terephthalate) and poly(ethylene isophthalate-*co*-ethylene terephthalate)s. In addition, differential scanning calorimetric measurements were conducted. Measurements were made both on polymers undergoing isothermal crystallization and during subsequent remelting. The primary and secondary crystallization behaviors are examined. Isophthalate units were found to be excluded from the crystals into amorphous layers during crystallization. No crystal thickening was observed during isothermal crystallization, which may be due to the relatively high chain rigidity. Secondary crystallization, detected predominantly at the later stages of crystallization, causes densification and shrinkage of the amorphous layer. Considering the results, it is proposed that secondary crystallization involves the formation of *short-range molecular order* in the amorphous layers of a lamellar stack as well as in the amorphous regions between lamellar stacks. This short-range-ordered phase has a lower density than the lamellar crystal formed by primary crystallization.

Introduction

A representative of semicrystalline polymers is poly(ethylene terephthalate) (PET), which is widely used as an engineering plastic material. The much investigated primary crystallization of PET was found to involve nucleation and growth.[1-7] In recent years, the secondary crystallization behavior of PET has also been studied.[1-17] As a result of such research efforts, several models have been discussed, particularly with respect to the secondary crystallization of PET polymer: (i) the thin lamellar stack insertion mechanism,[4,9-11] (ii) the single thin lamellar insertion mechanism,[8,12-14] (iii) the fringed micelle formation,[15-17] (iv) perfection of the crystals formed in the primary crystallization,[5,6] and (v) the positive edge-on branched lamellar stack formation mechanism.[2] Nevertheless, the secondary crystallization behavior of PET is still not fully understood; this subject needs more research and debate of researchers in both academia and industry. In contrast, the crystal growth of PET during primary crystallization has been studied in detail, providing an extensive database related to this process. However, there is lack of experimental data on the nucleation and growth of PET at the early stages of crystallization, the subject that needs further investigation.

 CCC 1022-1360/00/$ 17,50+.50/0

In the present work, small-angle X-ray scattering (SAXS) studies of such complex crystallization behavior are extended to poly(ethylene isophthalate-*co*-ethylene terephthalate) copolymers. Differential scanning calorimetry (DSC) investigations were also performed. The results of these studies are analyzed together with those for PET.

Experimental

Materials and sample preparation. Poly(ethylene terephthalate) and two poly(ethylene isophthalate-*co*-terephthalate) samples rich in ethylene terephthalate units synthesized in our laboratory were chosen for study, which are referred to as PET, 5IPT (4.9 mol-% isophthalate units), and 10IPT (9.8 mol-% isophthalate units) (see Fig. 1).[7]

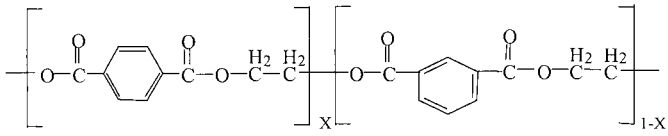

Fig. 1. Chemical structure of poly(ethylene isophthalate-*co*-ethylene terephthalate).

The molecular weight (M_w) was 36 000 for PET, 37 000 for 5IPT, and 36 000 for 10IPT.[7] The polymers were melt-molded under compression in a nitrogen atmosphere and cooled to room temperature, giving 2-mm thick sheets. These polymer sheets were cut either into disks of diameter 4 mm for use in X-ray scattering measurements, or into tiny pieces for use in DSC measurements.

Time-resolved SAXS measurements. SAXS measurements were conducted at the 4C1 SAXS beam line[18] of the Pohang Light Source facility with 2.5 GeV power at the Pohang University of Science and Technology, Korea. The X-ray radiation source has a wavelength of λ = 1.608 Å, and the beam size at the sample position was 0.6 x 0.6 mm. SAXS patterns were measured using a one-dimensional silicon-photodiode array detector (model X/PDA-2048, Princeton Instruments) consisting of 2048 pixels. A jumping hot-stage consisting of two independent chambers was employed. Each specimen was first melted for 5 min in the top chamber and then quickly transferred to the bottom chamber, which was held at the chosen crystallization temperature (T_c). The PET, 5IPT and 10IPT specimens were melted at 285 °C, 275 °C and 265 °C, respectively. The temperature of each chamber was controlled by a Eurotherm controller with a K-type thermocouple. The specimen chambers had nitrogen-blowing holes to protect the sample against thermal oxidation at high temperatures. To correctly monitor the sample temperature, a third Eurotherm controller was used that had a K-

type thin-wire thermocouple contacted directly to the specimen. The distance between sample and detector was 1.0 m. The scattering angle was calibrated with a collagen standard prepared from chicken tendon. SAXS measurements were carried out during isothermal crystallization over 170-240 °C and subsequent remelting at 3.0 °C/min. Each measurement was collected for 10 s. Each SAXS intensity profile was normalized to the incident X-ray beam intensity which was monitored by an ionization chamber placed in front of the sample, and corrected further for the background run.

The Lorentz-corrected SAXS profile was obtained as follows. The measured SAXS profile was extrapolated to q = 4 nm^{-1} by nonlinear least-square fitting of Porod's law,[19,20] giving the Porod constant and the constant scattering from density fluctuations. The SAXS profile was then treated by subtraction of the constant scattering from density fluctuations and corrected by multiplying by q^2, giving the Lorentz-corrected SAXS profile. The long period L (i.e., the mean distance between adjacent lamellae) was determined from the position (q_{max}) of the peak maximum in the Lorentz-corrected SAXS profile; q is given by $q = (4\pi/\lambda)\sin\theta$, where λ is the wavelength of the X-ray source and 2θ is the scattering angle. The Lorentz-corrected SAXS profile was inverse-cosine-Fourier-transformed to a one-dimensional correlation function $\gamma_1(z)$[21-23] where z is the direction perpendicular to the layer faces in the stack. Morphological parameters such as the lamellar crystal thickness d_c and the amorphous layer thickness d_a were determined from the normalized correlation function $\gamma_1(z)$.

In general, correlation function analysis can give the long period as well as the thickness (l_1) of one layer type (either the lamellar crystal layer or amorphous layer), according to the Babinet reciprocity. Thus, the other layer thickness (l_2) can be obtained from the long period and l_1. In the present study, l_1 is always smaller than l_2. We assign the thickness l_1 to the lamellar crystal thickness (d_c), and l_2 to the amorphous layer thickness (d_a). These assignments are in contradiction to those reported in the literature.[4,11,24] The reasons for this contradiction are as follows. First, the value of l_1 is larger for PET than for the copolymers crystallized under the same degree of supercooling. Instead, the value of l_2 is smaller for PET than for the copolymers. It is well known that noncrystallizable units incorporated into the polymer backbone have a strong tendency to be excluded from lamellar crystals. Thus, the copolymers should have thicker amorphous layers than PET.

In addition, invariant Q, which represents the total integrated scattering,[13,19,21] was obtained from the corrected SAXS profile. Q is related to the difference between the electron densities of the crystalline and noncrystalline regions (ρ_c-ρ_a), the volume fraction of lamellar stacks (φ_s), and the relative volume fraction of lamellae (φ_c) within the lamellar stack:[4,9,13]

DSC measurements. DSC thermograms were measured using a Seiko calorimeter calibrated with indium and tin standards. In the DSC measurements, all polymer samples were first melted and then heated to the chosen T_c, as described above for SAXS measurements. After isothermal crystallization, the crystallized samples were remelted using a heating rate of 3.0 °C/min. All measurements were made in nitrogen atmosphere.

Results and Discussion

Time-resolved SAXS measurements were conducted on PET, 5IPT and 10IPT during isothermal crystallization over a temperature range of 170-240 °C from the melt. Figures 2 and 3 show typical SAXS patterns measured during isothermal crystallization of 5IPT at a chosen temperature and subsequent remelting, respectively.

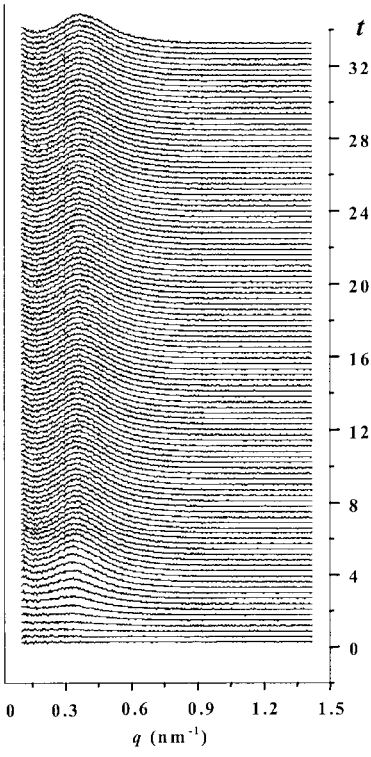

Fig. 2. Time-resolved SAXS patterns of 5IPT copolymer measured during isothermal crystallization at 216 °C for 60 min.

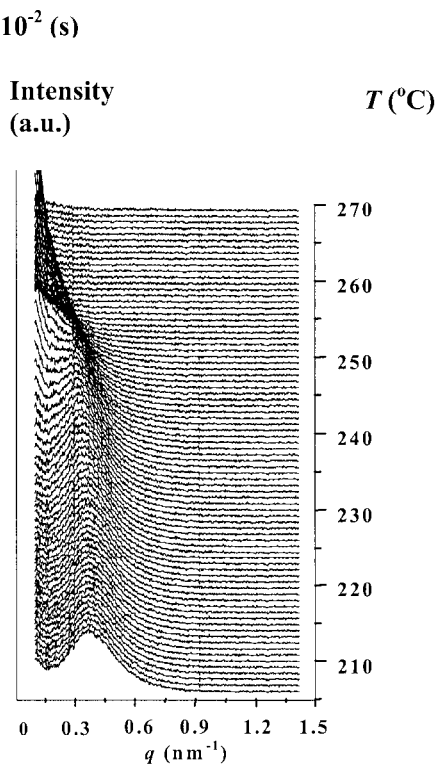

Fig. 3. Time-resolved SAXS patterns of 5IPT copolymer measured during heating at 3.0 °C/min after isothermal crystallization at 216 °C for 60 min.

As can be observed on a typical example in Fig. 2, in all the cases, the SAXS pattern is not detected in the beginning, but develops with the structural evolution associated with crystallization. With increasing crystallization time, the SAXS peak increases in intensity and its maximum shifts to the high-q region, remaining finally unchanged with a further increase in the crystallization time. In this study, the SAXS results are divided into two regimes according to the crystallization time: the primary and secondary crystallization regimes. The two regimes are divided approximately using the crystallization time ($t_{Q\max}$) at which the invariant Q reaches its maximum. The periods before and after this reference time are taken as the primary and secondary crystallization regimes, respectively.

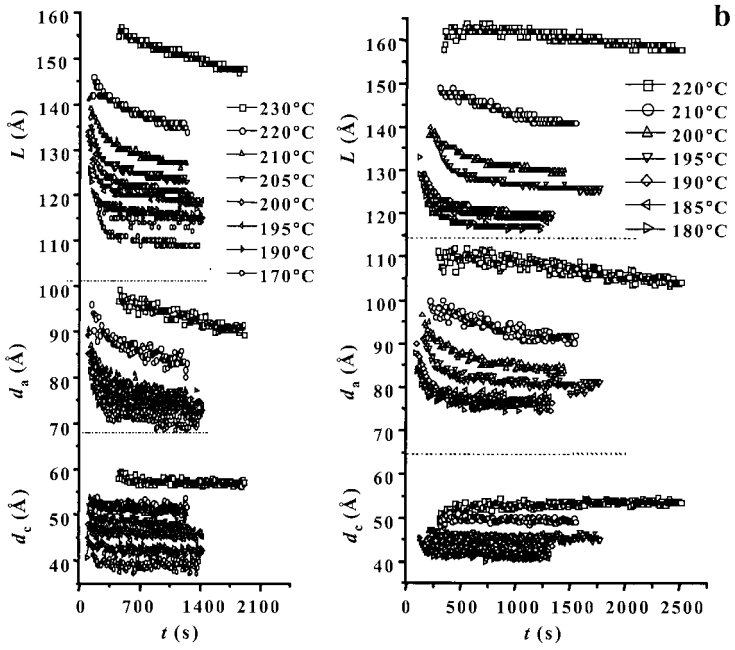

Fig. 4. Variation of morphological parameters (long period L, amorphous layer thickness d_a, and lamellar crystal thickness d_c) with time obtained from the time-resolved SAXS patterns measured during isothermal crystallization at various temperatures. (a) PET, (b) 5IPT.

Primary crystallization. Figure 4 shows the time dependence of morphological parameters (long period L, amorphous layer thickness d_a and lamellar crystal thickness d_c) obtained from the time-resolved SAXS patterns measured during isothermal crystallization of PET and 5IPT at various temperatures.

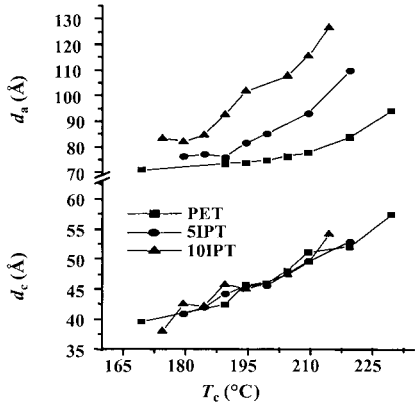

Fig. 5. Variations of amorphous layer thickness d_a and lamellar crystal thickness d_c with crystallization temperature in PET, 5IPT, and 10IPT. For each polymer, the morphological parameters were obtained from the SAXS pattern measured at $t = (t_{Q\max} + 100\ \text{s})$, where $t_{Q\max}$ is the time at which the invariant Q of the SAXS pattern reaches its maximum during crystallization.

Figure 5 illustrates the variations of d_c and d_a with isothermal crystallization temperature T_c, measured for PET and 5IPT crystallized for the time required for the invariant Q to reach a maximum ($t_{Q\max}$).

The lamellar crystal thickness d_c varies little with time in the crystallization of PET, indicating that no thickening occurred in the isothermal crystallization. A similar trend is observed for the crystallization of the copolymers. Furthermore, d_c varies little with the content of isophthalate units for systems crystallized at the same temperature. One can imagine that the kinked isophthalate units are included in the crystal formation at the early stages of crystallization and then excluded from the crystal at a later stage. If this were the case, the exclusion process would cause an increase in the density of the lamellar crystal and a decrease in the density of amorphous layer, leading to a large density difference between these layers. This density difference should cause an increase in the SAXS intensity profile and invariance at the later stages of crystallization. However, the SAXS results observed in this study show no such behavior. We therefore conclude that in the crystallization, lamellar crystals form and grow laterally without thickening and isophthalate units are excluded during this process.

The question remains as to why both the homopolymer and copolymers form lamellar crystals with almost the same value of d_c when crystallized at the same crystallization temperature. In fact, the copolymers have lower equilibrium melting temperatures T_m° than the

PET homopolymer.[7] Thus, taking into account only the degree of supercooling, one might expect the copolymers to make thicker lamellar crystals than the homopolymer. However, this behavior was not observed. Therefore, it is likely that the measured results are due to the restriction of crystallization by the kinked and relatively rigid isophthalate units.

In contrast, the value of d_a increases with increasing content of isophthalate units, even though the systems with different amounts of isophthalate crystallize at the same temperature. In addition, the difference between the d_a values of PET and its copolymer is large at higher isothermal crystallization temperatures. The increase in the thickness of the amorphous layers leads to a reduction in the crystallinity. This increase may be due to the exclusion of the kinked isophthalate units from lamellar crystals into the amorphous region.

In the isothermal crystallization runs the value of d_a decreases with time, regardless of polymer composition. Furthermore, d_a decreases more rapidly with time in the PET homopolymer than in the copolymers for systems crystallizing under the same degree of supercooling. There are two possible major factors that could account for the decrease in d_a during crystallization. The first factor is the distribution of the d_a values and its variation with time. The number of lamellae increases with time during stack building, which reduces the standard deviation in the d_a value and narrows its distribution. This has the effect of shifting the peak maximum of the SAXS profile into the high-q region.[25] The second factor is the relaxation of polymer chains in the amorphous layers. When lamellar stacks form, the polymer chains in the amorphous layers may be in a strained state. The strained polymer chains relax with time, which leads to a reduction in d_a.

Secondary crystallization. The change in the invariant Q with crystallization time was determined from the SAXS pattern measured during isothermal crystallization. A selection of the Q values obtained from PET and 5IPT is presented in Fig. 6.

In the results presented here, the value of Q is normalized by its maximum value. For PET, the value of Q is small and constant for an initial induction period; then increases rapidly with time up to a maximum at $t_{Q\max}$, after which it decreases slowly. This decrease in Q appears more clearly at the later stages of crystallization when the PET is quenched to a higher degree of supercooling. Similar Q variations are observed for the copolymers. The decrease in Q after $t_{Q\max}$ might be due to secondary crystallization taking place in addition to the primary crystallization. If secondary crystallization did not take place, Q would be expected to increase continuously with crystallization time because the continuation of primary crystallization would cause the density of the amorphous layers to decrease with time.

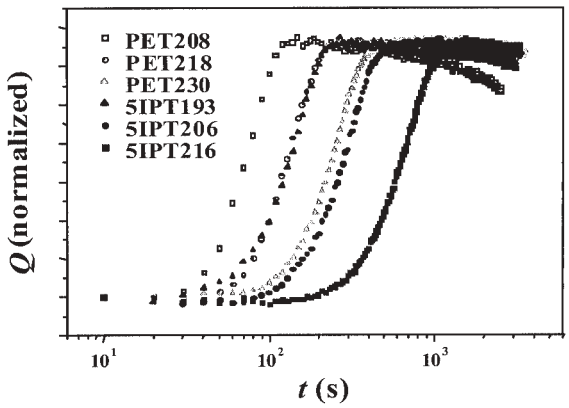

Fig. 6. Time dependence of invariant Q obtained from SAXS profiles measured during isothermal crystallizations of PET polymer and 5IPT copolymer at various temperatures (the codes indicate the polymer and its crystallization temperature).

To investigate the melting behavior of PET, 5IPT, and 10IPT, SAXS and DSC measurements were performed during the heating run at a rate of 3.0 °C/min after isothermal crystallization for 60 min at a temperature in the range 190-230 °C. In these experiments, 60 min was sufficient for both primary and secondary crystallization to occur. Representative results are shown in Fig. 7: the lamellar crystal thickness d_c and amorphous layer thickness d_a determined from the measured SAXS patterns are plotted together with the measured DSC thermograms.

In the DSC thermogram in Fig. 7a, the PET crystallized at 230 °C displays two major melting peaks: one peak in the high-temperature region with a very large heat of melting, and another peak in the low-temperature region. In general, lamellar crystals formed by primary crystallization are larger than those formed by secondary crystallization, causing them to melt in the high-temperature region. Thus, the peak in the high-temperature region can be assigned to the melting of crystals formed by primary crystallization. However, this melting endotherm may overlap either in part or fully with the exothermic peak of the recrystallization that may occur during heating.[2] The peak in the low-temperature region is assigned to the melting of the crystals formed by secondary crystallization. Similar melting behavior is observed for the 5IPT sample crystallized at 216 °C (see Fig. 7c).

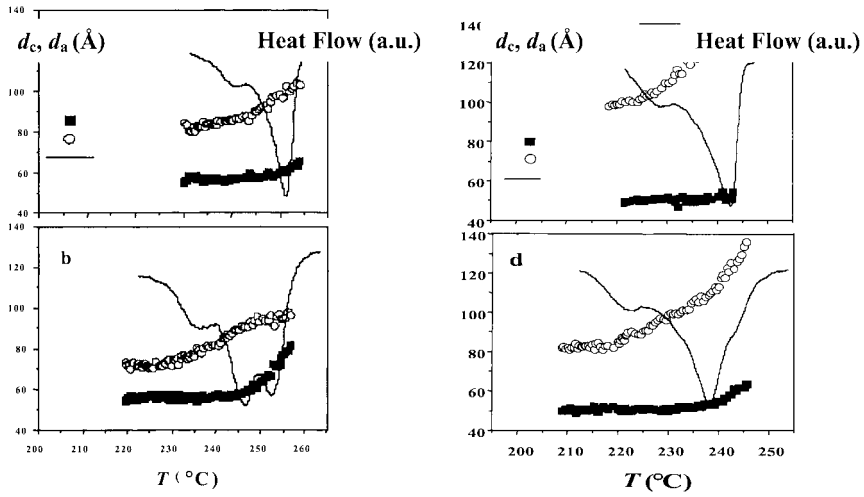

Fig. 7. DSC thermograms, as well as variations of amorphous layer thickness d_a and lamellar crystal thickness d_c with temperature, measured during heating at 3.0 °C/min after isothermal crystallization of a polymer for 60 min at various temperatures.
a PET230, *b* PET219, *c* 5IPT216, *d* 5IPT206 (the codes indicate the polymer and its crystallization temperature); d_c, d_a, heat flow.

In contrast to the results presented above, the PET crystallized at 219 °C shows three major melting peaks (see Fig. 7b). This polymer exhibits two melting peaks in the high-temperature region, rather than the single melting peak seen for PET crystallized at 230 °C. The peaks in the high-temperature region appear at around 247 °C and 253 °C, which fall on either side of the peak due to the lamellar crystals formed by primary crystallization at 230 °C. It is well known that thinner lamellar crystals form at lower crystallization temperatures, and that these crystals exhibit low melting points. We therefore assign the peak at around 247 °C to the melting of the lamellar crystals formed by the primary crystallization, and the peak at around 253 °C is assigned to the melting of crystals that recrystallized during the heating run. The melting point of the crystals from the secondary crystallization is also detected in this sample. The PET samples crystallized at 210-220 °C show a similar behavior to that described above, as do the 5IPT and 10IPT polymers crystallized at 190-210 °C (see an example in Fig. 7d).

From the DSC results presented above we find that the multiple melting points in the isothermally crystallized PET and its copolymers originate from the melting of the crystals formed by primary and secondary crystallization. In addition, it is noteworthy that the melting point of the recrystallized crystals is observed for PET and its copolymers crystallized at relatively high degrees of supercooling.

As displayed in Fig. 7, the value of d_c (which was determined from the measured SAXS pattern) in the heating run varies very little with temperature through the melting of the crystals formed by secondary crystallization, and continues to show little variation up to the temperature of the peak maximum corresponding to the melting of primarily formed lamellar crystals. This behavior was observed regardless of polymer composition and crystallization temperature. At higher temperatures, d_c increases rapidly with increasing temperature through the melting of the primarily formed and recrystallized crystals. The increase in d_c with temperature is particularly marked through the melting of the crystals formed by recrystallization during the heating run. This behavior is detected in samples crystallized with high degrees of supercooling.

In contrast, the value of d_a initially increases with temperature due to melting in the low-temperature region of the crystals formed by secondary crystallization. This behavior is observed regardless of polymer composition and crystallization temperature. With further increase in temperature, the increase in d_a becomes steeper due to the melting in the high-temperature region of the crystals formed by primary crystallization and recrystallization. The increase in d_a is larger in the copolymer than the homopolymer. Overall, d_a shows greater variations in the heating run than d_c. The relatively large variations in d_a are attributed to two main factors. First, the amorphous layer has a larger expansivity than the lamellar crystals, which makes a positive contribution to the expansion of d_a. The second factor is that the secondarily formed crystals melt in the low-temperature region, increasing the amorphous material proportion and causing the increase in d_a. The melting of the crystals formed by secondary crystallization contributes significantly to the expansion of d_a, even below the value of T_m for the crystals formed by primary crystallization. From these results we conclude that secondary crystallization causes PET and its copolymers to undergo densification.

Of the models mentioned earlier in the Introduction, both the thick and the thin lamellar stack insertion model[4,9-11] as well as the single thin lamellar insertion model[8,12-14] have been widely investigated. Continuing this trend, we consider the first two models and evaluate their validity for the secondary crystallization of PET and its copolymers investigated in this study. First, the thin lamellar stack insertion model predicts: (a) the SAXS profile to broaden and shift to the high-q region as crystallization proceeds and (b) Q to increase throughout the crystallization process, which is due to the overall crystallinity increased continuously by the formation of the thin lamellar stacks through secondary crystallization. Second, the single thin lamellar insertion model also predicts Q to always increase with crystallization time, which is due to the overall crystallinity increased by the formation of single thin lamellae, which have

the same electron density as the primarily formed lamellae, through the secondary crystallization.

However, the SAXS profiles and their Q variations found in the present study, as described above, are quite different from these predictions. Therefore, taking into consideration the results presented above, we propose a *new structural model* describing the amorphous layers in a lamellar stack and the amorphous regions between lamellar stacks, which become dense and shrink due to secondary crystallization. The proposed model involves a *short-range-ordered structure* that has a lower density than the lamellar crystals formed by primary crystallization. The *short-range-ordered structure* can consist of either single thin lamellae or a fringed micelle-like molecular order, which must have a lower density than the lamellar crystals formed by primary crystallization.

Conclusion

For 5IPT and 10IPT, the isophthalate units are excluded from the lamellar crystals into amorphous layers through the crystallization process. This exclusion leads to an increase in the amorphous layer thickness. However, PET and the copolymer systems crystallized at the same temperature form lamellar crystals with a similar thickness. This behavior might be due to the restriction of crystallization by the isophthalate units, which possess a kinked nature with some rigidity. The presence of isophthalate units lowers both the crystallization rate and crystallinity of the resulting polymer.

The crystal thickness is highly dependent on the crystallization temperature, showing that the degree of supercooling is the major driving force determining the thickness of lamellar crystals. However, no thickening occurs in the isothermal crystallizations, regardless of composition. Instead, the lamellar crystal undergoes perfectioning and lateral growth during the crystallization process, causing its melting temperature to shift to the high-temperature region. On the other hand, in the isothermal crystallization, the amorphous layer thickness d_a decreases with time, regardless of polymer composition. The reasons for the decrease in d_a have been considered, taking into account several factors possibly influencing the crystallization process.

Evidence of secondary crystallization is present in all the SAXS and DSC measurements for both the homopolymer and copolymers. Secondary crystallization causes densification of the amorphous layer, leading to a reduction in the amorphous layer thickness. This is strong evidence that secondary crystallization occurs mainly in amorphous layers. The melting point of the secondary crystals shifts to the high-temperature region with increasing crystallization

time. On the basis of these results, it is proposed that *the crystals formed by secondary crystallization form a short-range-ordered phase*. This short-range-ordered phase has a lower density than the lamellar crystals formed by primary crystallization.

Acknowledgements

This study was supported by the Korean Ministry of Science and Technology (MOST) (KISTEP - Basic Research Grant of Nuclear Energy) and by the Center for Integrated Molecular Systems (KOSEF). The synchrotron SAXS measurements were supported by MOST and POSCO.

References

1. S. W. Lee, B. Lee, M. Ree, *Macromol. Phys. Chem.*, **201**, 453 (2000).
2. F. J. Medellin-Rodriguez, P. J. Phillips, J. S. Lin, *Macromolecules*, **29**, 7491 (1996).
3. G. Hauser, J. Schmidtke, G. Strobl, *Macromolecules*, **31**, 6250 (1998).
4. Z.-G. Wang, B. S. Hsiao, B. B. Sauer, W. G. Kampert, *Polymer*, **40**, 4615 (1999).
5. P. J. Holdsworth, A. Turner-Jones, *Polymer*, **12**, 195 (1971).
6. U. W. Gedde, in *Polymer Physics*, Chapman & Hall, London, 1995, Chap. 7.
7. S. W. Lee, M. Ree, C. E. Park, Y. K. Jung, C.-S. Park, Y. S. Jin, D. C. Bae, *Polymer*, **40**, 7137 (1999).
8. A. M. Jonas, T. P. Russell, D. Y. Yoon, *Colloid Polym. Sci.*, **272**, 1344 (1994).
9. R. Verma, H. Marand, B. Hsiao, *Macromolecules*, **29**, 7767 (1996).
10. W. Wang, J. M. Schultz, B. S. Hsiao, *J. Macromol. Sci.: Phys.*, **37**, 667 (1998).
11. B. S. Hsiao, Z.-G. Wang, F. Yeh, Y. Gao, K. C. Z. Sheth, *Polymer*, **40**, 3515 (1999).
12. K.-N. Kruger, H. G. Zachmann, *Macromolecules*, **26**, 1756 (1993).
13. A. M. Jonas, T. P. Russell, D. Y. Yoon, *Macromolecules*, **28**, 8491 (1995).
14. C. Fougnies, P. Damman, D. Vollers, M. Dosiere, M. H. J. Koch, *Macromolecules*, **30**, 1385 (1997).
15. H. Marand, A. Alizadeh, R. Farmer, R. Desai, V. Velikov, *Macromolecules*, **33**, 3392 (2000).
16. B. Crist, E. S. Claudio, *Macromolecules*, **32**, 8945 (1999).
17. A. Alizadeh, L. Richardson, J. Xu, S. McCartney, H. Marand, Y. W. Cheung, S. Chum, *Macromolecules*, **32**, 6221 (1999).
18. J. Bolze, J. Kim, B. Lee, T. J. Shin, J.-Y. Huang, S. Rah, H. S. Youn, M. Ree, *Korea Polym. J.*, **9**, 450 (2001).
19. W. Ruland, *J. Appl. Crystallogr.*, **4**, 70 (1971).
20. J. T. Koberstein, R. S. Stein, *J. Polym. Sci.: Polym. Phys. Ed.*, **21**, 2181 (1983).
21. C. G. Vonk, G. Kortleve, *Colloid Polym. Sci.*, **220**, 19 (1967).
22. B. Goderis, H. Reynaers, M. H. J. Koch, V. B. F. Mathot, *J. Polym. Sci.: Polym. Phys. Ed.*, **37**, 1715 (1999).
23. G. R. Strobl, M. Schneider, *J. Polym. Sci.: Polym. Phys. Ed.*, **18**, 1343 (1980).
24. H. G. Zachmann, H. A. Stuart, *Makromol. Chem.*, **41**, 148 (1960).
25. R. Vignaud, J. M. Schultz, *Polymer*, **27**, 651 (1986).